

Experimental analysis of a semi-actively controlled steel building

Antonio Occhiuzzi[†] and Mariacristina Spizzuoco[‡]

*Department of Structural Analysis and Design, School of Engineering, University of Napoli Federico II,
Via Claudio n. 21 - 80125 Napoli, Italy*

(Received August 5, 2004, Accepted February 7, 2005)

Abstract. The strong need of verifying theories formulated for semi-active control through applications to real structures is due to the fact that theoretical research on semi-active control systems is not matched by a corresponding satisfactory experimental activity. This paper shows how a smart system including magnetorheological devices as damping elements can be implemented in a large-scale structural model, by describing in detail the kind of electronics (dedicated hardware and software) adopted during the experimental campaign. It also describes the most interesting results in terms of reduction of the seismic response (either experimental or numerical) of the semi-actively controlled structure compared to a passive operating control system, and in terms of the evaluation criteria proposed in the benchmark for seismically excited controlled buildings. The paper also explains how to derive from the classical theory of optimal control the adopted control logic, based on a clear physical approach, and provides an exhaustive picture of the time delays characterizing the control sequence.

Key words: semi-active control; magnetorheological dampers; large scale tests.

1. Introduction

The 11-storey steel Kyobashi Seiwa Building constructed in Tokyo, Japan, in 1989 was the first application of active structural control, and gave rise to a new stage in the field of innovative earthquake-resistant strategies for civil structures. Since then, different types of active, hybrid and semi-active control systems have been implemented in tens of buildings. An almost complete picture of the current state of control applications in Japan, the country having the largest number of applications in the world, is given in Nishitani and Inoue (2001). The authors provide a chronologically ordered list of the 32 controlled buildings in Japan, by specifying for each of them number of storeys, heights, locations, and type of actuators: 24 of them are high-rise buildings according to the Building Standard Law of Japan (buildings with heights of over 60 m). Due to their high flexibility and to the consequent relatively long natural period, they suffer the problem to become uncomfortable for occupants even during strong winds and moderate earthquakes, rather than showing issues related to the structural safety against severe earthquakes. 16% of the above structures (5 buildings) are equipped with Active Mass Driver (AMD) systems, 75% (24 buildings)

[†] Professor, Corresponding author, E-mail: antonio.occhiuzzi@unina.it

[‡] Researcher

with Hybrid Mass Dampers (HMD, i.e., a combination of TMD and AMD) systems, 3% (1 building) with an Active Variable Damper (AVD) system, 3% (1 buildings) with an Active Variable Stiffness (AVS) system, and the last 3% (1 building) with a combination of Base Isolation and AVD. Therefore, semi-active control has been applied only to 9% of the structures, i.e., 3 low-rise buildings. The authors explain that active structural control technology cannot be considered a viable strategy against severe earthquakes, and stress the importance of further research and development of semi-active control systems representing the most promising strategies based on the principle of less energy and better performance. Therefore, semi-active control is actually recognized by the structural community as a powerful tool for protecting building and bridge structures subjected to strong external excitations such as large earthquakes (Symans and Constantinou 1999, Kobori 2002, Jung *et al.* 2004), and is the subject of increasing research efforts both from theoretical and experimental perspective.

A semi-active control device is typically a “smart” passive device able to self-adjust its own mechanical properties in real time according to properly selected control algorithms, which represent the operational logic driving the device’s instantaneous behaviour on the base of the structural response and/or the external dynamic excitation. The ability of modifying the parameters of a device provides a semi-active control system the capability to produce a temporary variation of the stiffness and/or damping characteristics of the structure in order to maximize the dissipated energy and to eliminate the possibility of resonance. In practice, a semi-active control device is able to apply even large control forces with a much smaller energy supply compared to fully active control. Furthermore, being typically small and compact, it can be simply installed in a structure pretty much like a passive control device and, due to its reactive behaviour, it cannot drive the hosting structure to dynamic instability making the controlled system highly reliable. Finally, its maintenance is much easier compared to active control devices such as force actuators.

In the field of civil structures, the need to validate the concepts presented above through real-scale experimental activities is now perceived as urgent. The results of stationary excitation tests and free vibration tests on an actual Japanese low-rise (11 storeys) building, equipped with semi-active switching oil dampers included in bracing systems, are shown by Tagami *et al.* (2002). The experimental tests, executed in both the ‘uncontrolled’ and the ‘controlled’ structural conditions, showed that semi-active dampers can increase the building overall damping, and that the response reduction effect can be almost twice as much that associated to their passive counterparts. Besides, the semi-active viscous devices were able to operate even for very small values of the stroke, i.e., they could control vibrations caused not only by large earthquake but also by small earthquakes or strong wind.

Another full-scale application (Yamamoto *et al.* 2002) is the installation of two semi-active mass dampers in a Japanese high-rise (24 storeys) steel building, whose upper floors are subjected to uncomfortable vibrations especially in the rotational direction due to strong winds. The mass damper system, using a viscous damper semi-actively controlled by solenoid valves in the hydraulic circuit, has been designed to be effective also during large earthquakes inducing large stroke displacements and velocities. Indeed, the solenoid valves can provide the optimum damping factor of the control system for smaller vibrations under strong winds, and an higher damping factor when larger vibrations occurs under the action of serious earthquakes.

Among recent experimental applications performed on building mock-ups, the base-isolated 1:4-scale 3-story steel building frame, studied and tested by Wongprasert and Symans (2002), has to be mentioned. The results of the shaking table tests carried out on the frame mock-up equipped with

the smart isolation system, made up of spherical sliding bearings combined with variable fluid dampers, compared to those of the corresponding passive isolation system, revealed that the variable dampers are effective in controlling the dynamic response of the superstructure while simultaneously bounding the deformation of the isolation system. The performance of the isolation system was evaluated by using both near and far-field historical earthquake records as ground excitation. However, its effectiveness was limited because of the relatively high bearing coefficient of friction which resulted in infrequent sliding of the bearings, and thus activation of the dampers.

A 3-story large-scale test frame was experimentally investigated by Hiwatashi *et al.* (2002) either with a base isolation system, made up of four laminated rubber bearings and a semi-active magnetorheological (MR) damper, or with a semi-active MR damper installed through K-type braces at the first story in the center structure plane. It is shown that, in the second control configuration, the structural response, in terms of displacement and acceleration, obtained under the input waves used for the shaking table tests (a sweep sinusoidal wave, white noise wave and different earthquake waves), decreases with the rise of the electrical current to the MR damper.

Another experimental application with a variable-damping device using MR fluids was made by Morishian *et al.* (2002) on a 3-story small ($100 \times 200 \times 660$ mm) structural mock-up, where the device is inserted between the top of a brace and the first floor. A sine-sweep excitation test, with frequency slowly increasing from 2 to 20 Hz, showed the performance of the vibration control system in terms of reduction of floor's displacements.

Control systems based on the rheological properties of MR fluids are making their way also in real structures. Chen *et al.* (2004) describe how the adoption of MR dampers on the Dongting Lake cable-stayed bridge (China) is effective in dramatically reducing wind induced vibrations of the stays. Furthermore, the adoption of MR dampers in two buildings in Japan is described in Spencer and Nagarajaiah (2003).

However, even if some applications of semi-active control techniques and technologies can be found in literature (really few when dealing with full-scale structures), there are some practical important issues which the actual knowledge has not yet solved, related to the whole implementation process, including overall system configuration, software/hardware integration, system status monitoring, measures and control performance verification. From a different perspective, an attempt to bridge the theory-to-implementation gap by handling and solving the many problems involved in the transition from a theoretical control system to a real one, has been made by Chu *et al.* (2002). The authors lay stress on the fact that setting up a control system is a time consuming and costly process, often based on a trials and errors iterative process, hardly compatible with laboratories schedules, and therefore they propose a real-time integrated testing platform. Such a platform is based on the idea of generating the real-time response of a structure under external loading (wind or earthquake) with the interaction of the control force generated by the controller in real time. The platform is composed by a Signal Interface System, a Digital Signal Processing controller, and a Real-time Structural Simulator. The first component, serving as a link between the second and third ones, depends on the devices which generate the control forces, the type of measuring equipment, and the specification of the data acquisition/conversion systems. It includes conditioning, filtering, monitoring, limitation detection and signal communication. The Digital Signal Processing controller is a dedicated computer which calculates the control force through the properly chosen and implemented control algorithm. It contains a processor, a converter board with input channels and a converter board with output channels. The digital Real-time Structural Simulator has the aim to reproduce in real time the signals of the test structure's response, and uses a personal computer

equipped with a digital acquisition board. In practice, when testing the performance of a control system, two real time processors are needed: the first one simulates the structural behaviour under the action of the external disturbance, and the second one provides the control forces according to the response fed-back by the first processor. The idea of the authors allows to face almost all the problems occurring in the implementation of a structural control system before the true final simulation with the real structure, thus permitting a considerable time reduction and economic saving.

The analysis of the available scientific literature leaves, however, some unanswered issues:

- It is quite difficult to understand the kind of equipment adopted in the experimental tests described and, above all, its complexity.
- How big is the step, still to be made, to bring a semi-active control system outside of a lab and to real-life applications?
- How large is the qualitative and quantitative improvement in the reduction of the structural response associated to semi-active control systems compared to their passive counterparts?

From this perspective, this paper describes the experimental campaign designed in order to deal with the items listed above.

The experimental tests presented in the following sections have been built around 4 available prototype magnetorheological (MR) dampers. Among the different kinds of recently investigated semi-active devices, MR dampers can effectively represent the materialization of the concept of time-varying damping device. In fact, a semi-active MR damper is characterized by the possibility of continuously varying the intensity of the magnetic field inside its body by using low-power electrical currents, so that a wide range of physical behaviors can be commanded to the device (Yang *et al.* 2002). The operation of such devices is fast (in the order of few milliseconds) and reliable because of the dependence of their self-adjusting properties on electrical rather than mechanical modifications inside the devices (Occhiuzzi *et al.* 2003). The experimental campaign described in the following has been designed so as to verify the effectiveness of a properly manufactured semi-active control system based on MR dampers for a steel structure.

2. Experimental set-up

2.1 The tested structure

In the framework of the EU funded SPACE (Semi-active and PAssive Control of the dynamic behaviour of structures subjected to Earthquakes, wind and vibrations) research project (5th FP, 1998-2002), a large scale steel frame mock-up (named MISS), equipped with four semi-active bracing systems (Fig. 1), has been the object of an experimental campaign performed on the 6 degrees of freedom Multi Axes Shaking Table for Earthquake Reproduction (of 4×4 m dimensions) located at the Structural Dynamics Testing Laboratory of ENEL.Hydro – ISMES in Bergamo, Italy (Medeot *et al.* 2001, Serino *et al.* 2002).

The MISS structure is a 4-story steel frame composed by 4 horizontal frames (3.3×2.1 m plan dimensions) manufactured using HEB100 beam elements and bolted with an inter-story distance of 0.9 m at 6 vertical columns (HE100B) 4.5 m high. Each floor slab supports 4 concrete masses, each weighting 12.8 kN. The total weight of the structure is 226 kN. The steel grade is 275J0H (Italian classification Fe430, characteristic ultimate strength $f_{tk} = 430$ MPa, characteristic yield strength $f_{yk} = 275$ MPa and Young's modulus $E_s = 206$ GPa).



Fig. 1 MISS steel frame structure

The circular frequencies of the structure along the short edge direction, $\omega_{1, \text{exp}} = 13.82 \text{ rad/s}$, $\omega_{2, \text{exp}} = 54.66 \text{ rad/s}$, $\omega_{3, \text{exp}} = 117.50 \text{ rad/s}$, have been derived from the experimental results of the sinusoidal single axis sweep tests performed to characterize the uncontrolled structure.

The 4 degrees of freedom plane model able to reproduce the first four transversal modes of the uncontrolled building (i.e., without any bracing system) is characterized by the following equation of motion, where the base acceleration $\ddot{x}_g(t)$ represents the input excitation of the system and \mathbf{i} is a vector with all unity elements:

$$\mathbf{M}_s \cdot \ddot{\mathbf{x}}_s(t) + \mathbf{C}_s \cdot \dot{\mathbf{x}}_s(t) + \mathbf{K}_s \cdot \mathbf{x}_s(t) = -\mathbf{M}_s \cdot \mathbf{i} \cdot x_g(t) \quad (1)$$

The diagonal mass matrix (m_{f1} , m_{f2} , m_{f3} , m_{f4} represent the masses of the floors), the full stiffness matrix and the proportional damping matrix have been obtained on the basis of the tests performed in the uncontrolled configuration:

$$\mathbf{M}_s = \begin{bmatrix} m_{f1} & 0 & 0 & 0 \\ 0 & m_{f2} & 0 & 0 \\ 0 & 0 & m_{f3} & 0 \\ 0 & 0 & 0 & m_{f4} \end{bmatrix} = \begin{bmatrix} 5,679 & 0 & 0 & 0 \\ 0 & 5,679 & 0 & 0 \\ 0 & 0 & 5,679 & 0 \\ 0 & 0 & 0 & 5,679 \end{bmatrix} \text{ [kg]}$$

$$\mathbf{K}_s = \begin{bmatrix} k_{11} & k_{12} & k_{13} & k_{14} \\ k_{21} & k_{22} & k_{23} & k_{24} \\ k_{31} & k_{32} & k_{33} & k_{34} \\ k_{41} & k_{42} & k_{43} & k_{44} \end{bmatrix} = \begin{bmatrix} 110754.0 & -63347.4 & 20153.3 & -2772.9 \\ -63347.4 & 83565.0 & -55312.2 & 14074.6 \\ 20153.3 & -55312.2 & 66792.6 & -27785.7 \\ -2772.9 & 14074.6 & -27785.7 & 15951.1 \end{bmatrix} \text{ [kN/m]}$$

$$\mathbf{C}_s = 2\alpha\mathbf{K}_s + 2\beta\mathbf{M}_s \quad \text{[kNs/m]} \quad (2)$$

where the coefficients $\alpha = 0.3978 \cdot 10^{-3} \text{ s}$ and $\beta = 0.2585 \text{ s}^{-1}$ have been derived by considering the damping ratio 2.5% experimentally observed for the first two transversal modes.

From the above matrices, the following modal frequencies and corresponding eigenvectors have been obtained:

$$\omega_1 = 13.07 \text{ rad/s}, \omega_2 = 49.83 \text{ rad/s}, \omega_3 = 114.67 \text{ rad/s}, \omega_4 = 183.09 \text{ rad/s}$$

$$\begin{array}{cccc} \phi_1 & \phi_2 & \phi_3 & \phi_4 \\ \begin{bmatrix} -0.1006 & 0.2777 & -0.5745 & 0.6033 \\ -0.3126 & 0.5061 & -0.1520 & -0.6173 \\ -0.5326 & 0.1991 & 0.5225 & 0.4050 \\ -0.7124 & -0.4281 & -0.2576 & -0.1244 \end{bmatrix} & & & \end{array} \quad (3)$$

which show a satisfactory agreement with the experimental results.

The above linear continuous-time 4th-order system can be represented in the state space as follows:

$$\dot{\mathbf{z}}_s(t) = \mathbf{A}_s \mathbf{z}_s(t) + \mathbf{e}_s \ddot{x}_g(t) \quad (4)$$

where $\mathbf{z}_s(t)^T = [\mathbf{x}_s(t)^T \ \dot{\mathbf{x}}_s(t)^T]$ is the 8-dimensional state vector ($\mathbf{x}_s(t)$ and $\dot{\mathbf{x}}_s(t)$ are the relative displacements and velocities of the 4 DOFs of the system) and the matrices of the system are:

$$\mathbf{A}_s = \begin{bmatrix} \mathbf{O}_{4 \times 4} & \mathbf{I}_{4 \times 4} \\ -\mathbf{M}_s^{-1} \mathbf{K}_s & -\mathbf{M}_s^{-1} \mathbf{C}_s \end{bmatrix}_{8 \times 8}, \quad \mathbf{e}_s = \begin{bmatrix} \mathbf{O}_{4 \times 1} \\ -\mathbf{i}_{4 \times 1} \end{bmatrix}_{8 \times 1} \quad (5)$$

2.2 The semi-active bracing system

Steel frames are well suited to host bracing elements to resist lateral forces, therefore a “smart” bracings system seems to be quite effective in such structures (Occhiuzzi and Spizzuoco 2003). The proposed semi-active (“smart”) bracing system is made up by three parts: an elastic brace, a semi-active device representing the time-varying damping element linking the brace to the hosting structure, and a control algorithm.

Along the short edge (transverse) direction of the frame, 4 flexible braces made of steel profile IPE200, each equipped on the top with a semi-active MR damper (Fig. 2), have been mounted between ground and second floor (the lower ones) and between second and fourth floor (the upper ones). The bracing stiffnesses have been chosen of the same order of magnitude of the lateral stiffnesses of the frame in order to optimize the effectiveness of the semi-active control system (Inaudi 2000). In order to obtain these stiffnesses, the free length of the braces has been reduced by inserting reinforcing plates at the base.

Within the research project SPACE, the semi-active MR dampers have been designed and manufactured by Maurer Söhne (Munich, Germany), and experimentally tested to evaluate the characteristics of their operations (Fig. 3). They look pretty much like conventional fluid viscous damper, with the exception of some extra wiring needed to feed the coils inside the body. The absence of moving parts like electrically controlled valves or mechanisms make them very reliable

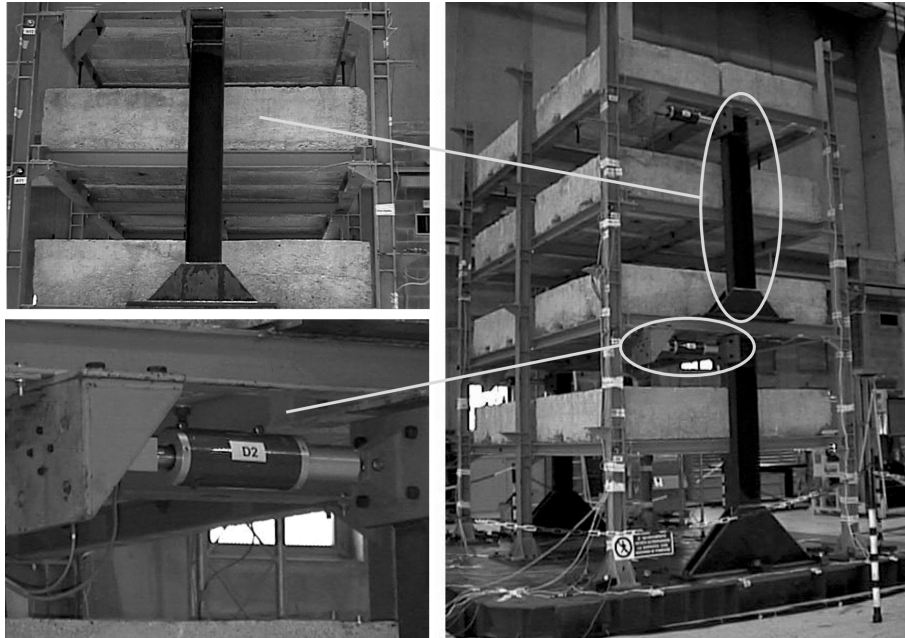


Fig. 2 Elastic brace and MR damper in MISS structure



Fig. 3 The prototype MR dampers

with respect to other semi-active devices. Each prototype MR device has overall dimensions $712 \times 200 \times 250$ mm and a mass, without connections, approximately equal to 16 kg; it can develop a maximum damping force of 50 kN along its longitudinal axis and the piston stroke is equal to ± 25 mm. The magnetic field produced in the device is generated by a magnetic circuit implemented in a very innovative way, and the current in the circuit, provided by a power supply commanded by a voltage input signal, is in the range $i = 0\sim 3$ A.

A wide experimental campaign carried out on these dampers has demonstrated that the classical linear Bingham model, commonly considered in literature to describe their dynamical behaviour, shows certain limits if used for different current levels i and test frequencies. The following numerical “improved model” (Occhiuzzi *et al.* 2003):

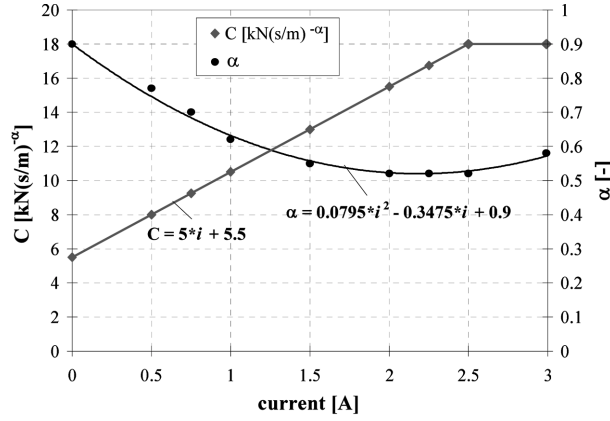


Fig. 4 Improved model: constitutive laws of the viscous component's parameters

$$F_d(U) = F_\eta + F_{dy} = C(i) \cdot |U|^{\alpha(i)} \cdot \text{sgn}(U) + [F_{dy,\min} + (F_{dy,\max} - F_{dy,\min}) \cdot i/i_{\max}] \cdot \text{sgn}(U) \quad (6)$$

has turned out to closely fit the experimental data measured during the tests on the MR dampers. That is, the total force in the MR damper can be expressed as sum of two components due to the fluid viscosity and to the magnetic field-induced yield stress, respectively. According to the experimental characterization of the devices, both components depend on the current intensity in the coils inside the body of the damper. The first component (F_η) has to be assumed non-linearly dependent on the relative velocity U between the damper's ends in order to take into account the dependence of the damper's behaviour on the test velocity (Fig. 4): the tests on the devices have shown that the viscous damping parameter C is linearly variable with the current in the coils inside the damper ($C(i) = 5.5 + 5.0 \cdot i$ [kNs/m]) and the power α is a quadratic function of the current i ($\alpha(i) = 0.0795 \cdot i^2 - 0.3475 \cdot i + 0.9$). The second component (F_{dy}) is given by a linear relationship with the current i and varies from a minimum value $F_{dy,\min} = 0.6$ kN (at $i = 0$ A) due to the friction force of the gaskets to a maximum value $F_{dy,\max} = 28$ kN (at $i_{\max} = 3$ A) due to magnetic saturation.

As regard the promptness of the semi-active MR dampers, a statistical analysis of the experimental results of semi-active shaking table tests, performed by using a dedicated electronics, has shown that the delays of the control chain (acquisition-processing-actuation) are practically independent on the test frequency and their mean values are about 10 ms in the on-off phase (i.e., after a switch off command to the device, current i from 3 A to 0 A) and about 13 ms in the off-on phase (i.e., after a switch on command to the device).

In the 6 (4 + 2) DOF plane model representing the controlled building (i.e., with the bracing systems), the last 2 dynamic degrees of freedom correspond to the moving masses of the "smart" bracing systems, i.e., the moving masses m_{bl} of the lower assemblies (brace + MR damper) and m_{bu} of the upper ones. The values $m_{bl} = m_{bu} = 2 \times 170$ kg include the mass of the two devices located at a same level, the participating moving mass of the two lower and upper braces, respectively, and the mass of the different connections and reinforcements. Finally, the global stiffnesses of the braces at the lower and upper level, respectively $k_{bl} = 2 \times 4400 = 8800$ kN/m and $k_{bu} = 2 \times 1755 = 3510$ kN/m, have been calculated accounting for the deformability of the reinforcing plates and the bolted connections, and for the compliance of the horizontal beams which the bottom of the upper level braces are connected to.

As regard the MR damper, the “improved model” expressed in Eq. (6) has been assumed to simulate its mechanical behaviour, so that the modelling of the variable-damping bracing system is characterized by the following five mechanical parameters: the moving mass m_b of the semi-active system, the stiffness k_b of the elastic brace, the viscous coefficient C of the MR damper “improved model”, the power α of the velocity in the MR damper’s viscous component, and the magnetic field-induced threshold F_{dy} in the MR damper’s friction component.

Therefore, the 6-DOF plane model is characterized by the following equation of motion:

$$\mathbf{M} \cdot \ddot{\mathbf{x}}(t) + \mathbf{C} \cdot \dot{\mathbf{x}}(t) + \mathbf{K} \cdot \mathbf{x}(t) = -\mathbf{M} \cdot \mathbf{i} \cdot x_g(t) + \mathbf{a}\mathbf{l} \cdot \mathbf{u}(t) \tag{7}$$

whose vectors and matrices become:

$$\mathbf{x} = \begin{bmatrix} x_{f1} \\ x_{f2} \\ x_{f3} \\ x_{f4} \\ x_{bl} \\ x_{bu} \end{bmatrix}, \quad \mathbf{u} = \begin{bmatrix} F_{d,l}^s \\ F_{d,u}^s \end{bmatrix}, \quad \mathbf{i} = \begin{bmatrix} 1 \\ 1 \\ 1 \\ 1 \\ 1 \\ 1 \end{bmatrix}, \quad \mathbf{a}\mathbf{l} = \begin{bmatrix} 0 & 0 \\ 1 & 0 \\ 0 & 0 \\ 0 & 1 \\ -1 & 0 \\ 0 & -1 \end{bmatrix}, \quad \mathbf{M} = \begin{bmatrix} m_{f1} & 0 & 0 & 0 & 0 & 0 \\ 0 & m_{f2} & 0 & 0 & 0 & 0 \\ 0 & 0 & m_{f3} & 0 & 0 & 0 \\ 0 & 0 & 0 & m_{f4} & 0 & 0 \\ 0 & 0 & 0 & 0 & m_{bl} & 0 \\ 0 & 0 & 0 & 0 & 0 & m_{bu} \end{bmatrix}$$

$$\mathbf{K} = \begin{bmatrix} k_{11} & k_{12} & k_{13} & k_{14} & 0 & 0 \\ k_{21} & k_{22} + k_{bu} & k_{23} & k_{24} & 0 & -k_{bu} \\ k_{31} & k_{32} & k_{33} & k_{34} & 0 & 0 \\ k_{41} & k_{42} & k_{43} & k_{44} & 0 & 0 \\ 0 & 0 & 0 & 0 & k_{bl} & 0 \\ 0 & -k_{bu} & 0 & 0 & 0 & k_{bu} \end{bmatrix}, \quad \mathbf{C} = \begin{bmatrix} \mathbf{C}_s & \mathbf{O}_{4 \times 2} \\ \mathbf{O}_{2 \times 4} & \mathbf{O}_{2 \times 2} \end{bmatrix} \tag{8}$$

$F_{d,l}^s$ and $F_{d,u}^s$ are the damping forces considered acting on the main structure, i.e., of opposite sign with respect to the forces $F_{d,l}$ and $F_{d,u}$ acting on the MR dampers.

In the state space the above structural linear 6th-order system has the following form:

$$\dot{\mathbf{z}}(t) = \mathbf{A}\mathbf{z}(t) + \mathbf{e}\ddot{x}_g(t) + \mathbf{B}\mathbf{u}(t) \tag{9}$$

where $\mathbf{z}(t)^T = [\mathbf{x}(t)^T \ \dot{\mathbf{x}}(t)^T]$ is the 12-dimensional state vector ($\mathbf{x}(t)$ and $\dot{\mathbf{x}}(t)$ are the relative displacements and velocities of the 6-DOF system) and $\mathbf{u}(t)$ is the 2-dimensional vector of the control forces acting on the main structure. The matrices of the system are:

$$\mathbf{A} = \begin{bmatrix} \mathbf{O}_{6 \times 6} & \mathbf{I}_{6 \times 6} \\ -\mathbf{M}^{-1}\mathbf{K} & -\mathbf{M}^{-1}\mathbf{C} \end{bmatrix}_{12 \times 12}, \quad \mathbf{B} = \begin{bmatrix} \mathbf{O}_{6 \times 2} \\ -\mathbf{M}^{-1}\mathbf{a}\mathbf{l} \end{bmatrix}_{12 \times 2}, \quad \mathbf{e} = \begin{bmatrix} \mathbf{O}_{6 \times 1} \\ -\mathbf{i}_{6 \times 1} \end{bmatrix}_{12 \times 1} \tag{10}$$

2.3 Instrumentation and dedicated electronics

During the experimental campaign performed on the controlled MISS structure, the shaking table has been driven only along the transversal direction of the frame (X). Two separate sets of hardware have been utilized for the acquisition of the structural response and for the control system.

Tables 1 and 2 list, respectively for the structural response and the control system, the channels acquired during the experiments, the instrumentation used and the measured physical quantities, whereas the sketch in Fig. 5 show the experimental set-up of the building, i.e., the position of the

Table 1 Sensors for the response acquisition: acquisition channels, transducers and measured physical quantities

Channel	Transducer	Physical quantity acquired
ATx, ATy, ATz	Accelerometer	Accelerations of shaking table
A1~A12	Accelerometer	Accelerations of the floors (X and Y directions)
R1x	LVDT	2nd floor displacement relative to the shaking table
P1, P2	Voltage transd.	Voltage commanding the upper and lower devices
C1~C4	Current transd.	Current supplied to the devices
LD1~LD4	LVDT	Relative displacements in the dampers
FD1~FD4	Load cell	Axial forces on dampers piston

Table 2 Sensors for the control system: acquisition channels, transducers and measured physical quantities

Channel	Transducer	Physical quantity acquired
AT	Accelerometer	Acceleration of shaking table
AC1~AC4	Accelerometer	Accelerations of the floors (X direction)
LD1~LD4	LVDT	Relative displacement in the dampers
FD1~FD4	Load cell	Axial force on dampers piston

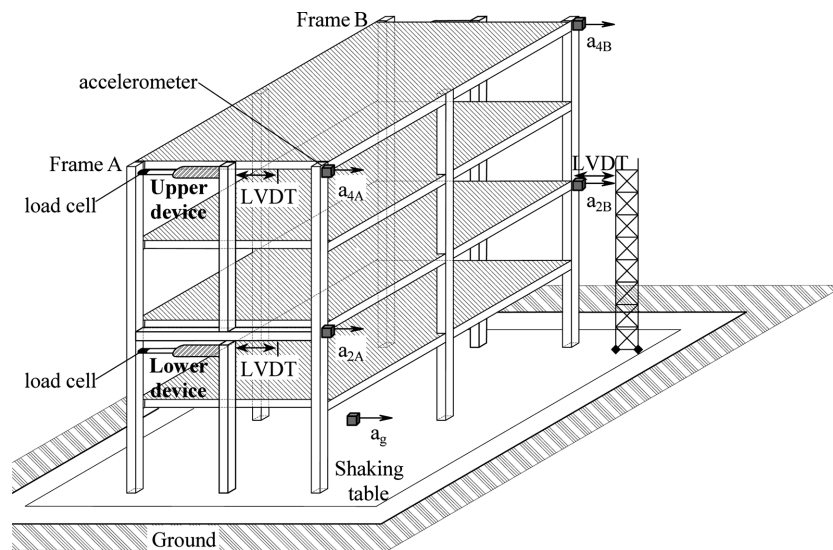


Fig. 5 Experimental set-up

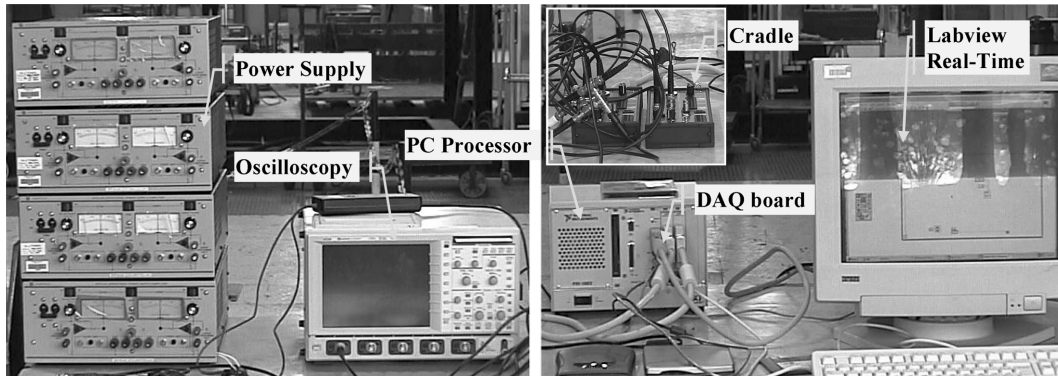


Fig. 6 Dedicated electronics for semi-active tests

most significant transducers on the shaking table and on the structure. It is worth to make clear that the relative displacement between the MISS 2nd floor and the shaking table has been measured by using a rigid reference structure.

For the semi-active operation of the MR dampers, a specific electronic hardware and software (Fig. 6) has been used, consisting of a real time National Instruments CPU (Pentium III, 850 MHz), two digital acquisition boards (DAQ boards) with a total of 16 inputs and 4 outputs (16 bits resolutions and 333 kHz sampling rate), the environment Labview Real-Time (National Instruments 2000) able to extend the Labview graphical programming to create applications with deterministic real-time performance, and four operational power supplies from Kepco Inc. (New York, USA), model BOP 50-4M. They are fully dissipative linear stabilizer for laboratory and systems applications, each having two bipolar control channels (voltage and current mode), selectable and individually controllable either from its front panel controls, or by remote signals. They have an output power of 200 W, a maximum input power of 450 W, and an output range of ± 50 V.

In order to limit to few milliseconds the time needed to reach the steady-state phase of the current inside the dampers' electromagnetic circuit, the power supplies have been used according to a current-driver scheme rather than a voltage-driver one. In fact, preliminary tests on the semi-active operation of the MR dampers have clearly showed that, in the case of a current driven feeding scheme, a sudden change (from 0 to 7.5 V) of the voltage driving signal to the power supply makes the voltage difference at the edges of the coils reach, for a short time, a value near the saturation ($\cong 50$ V) and, subsequently, the voltages settles down to a stable value of 11 V. At the same time, the current inside the damper rises in about 7 ms from 0 to the maximum value ($\cong 3$ A). Similarly, when the control command voltage steps down from 7.5 to 0 V, a negative voltage spike of about -50 V can bring the current down from 3 to 0 A in about 5 ms. The positive effect of the current driving powering method is discussed in the following section "Analysis of the experimental results".

3. Control algorithm and its implementation

In order to be capable of self-adjusting their own mechanical properties in real time according to a desired final effect, semi-active devices need an operational logic, i.e., a control algorithm, which

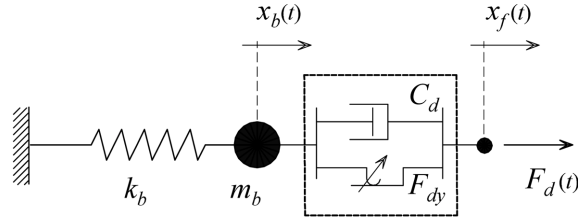


Fig. 7 Variable-damping bracing system with MR device

drives their instantaneous behaviour. Classical control algorithms have been developed in scientific fields different than structural engineering and, therefore, it is often not viable to apply a given standard algorithm “as is”.

A simple, yet effective control logic for a variable-damping bracing system (VDB) was proposed by Inaudi and Hayen (1995) in the case of a time-varying linear viscous damping device, and has been modified by the authors (Occhiuzzi and Serino 2002) in order to be applied to the case of a MR device with a time-varying magnetic field-induced plastic threshold (Fig. 7). The control logic is intended to maximize the extraction of energy from the main structure, by keeping locked the VDB’s MR damper during most of the operating time in order to transfer energy from the structure to the elastic brace, and unlocking it for short time intervals when the energy stored in the elastic element is dissipated by the damper. These short intervals begin immediately after a relative minimum or maximum in the motion $x_f(t)$ of the points of attachment of the VDB on the hosting structure. For a proper operation of the control system, the VDB system must have a natural frequency much higher than that of the controlled structure and a damping behaviour during unlocking intervals so as to achieve a fast energy dissipation. On the other hand, during locking phases the damping behaviour of the VDB system must be selected quite large so that the VDB’s deformation occurs mostly in the spring.

The analytical formulation of this control logic:

$$\begin{aligned} \text{if } F_d(t) \cdot \dot{x}_f(t) > 0 \quad \text{then } F_{dy}(t) &= F_{dy, \max} \\ \text{if } F_d(t) \cdot \dot{x}_f(t) < 0 \quad \text{then } F_{dy}(t) &= F_{dy, \min} \end{aligned} \quad (11)$$

contains the product of the damper’s force $F_d(t)$ by the structural velocity $\dot{x}_f(t)$, i.e., the power flow from the main structure to the semi-active bracing system. $F_{dy, \max}$ and $F_{dy, \min}$ are the selectable damping values of the 2-stage MR device. During the storing phases, corresponding to time intervals when the power flow from the structure to the control system is positive, the VDB has to be tuned so as to achieve the maximum possible strain in the elastic element. Therefore, the value of the variable plastic threshold F_{dy} , controllable by the applied magnetic field and, in turn, by the current intensity feeding the semi-active device, has to be set as high as possible. When the sign of the power flow changes to negative, by switching F_{dy} to its minimum value the dissipation phase is invoked to let the MR damper dissipate the elastic energy stored in the brace. If the control system is properly designed, the strain of the brace goes fast to zero and the elastic energy stored therein is dissipated in a time interval that is short if compared to the natural period of the hosting frame.

The implementation of the control logic to the tested structure is expressed by the following two relations for the lower and upper devices, respectively:

$$\begin{aligned} \text{if } F_{d,l}(t) \cdot \dot{x}_{f2}(t) > 0 \quad \text{then } F_{dy,l}(t) &= F_{dy, \max} \\ \text{if } F_{d,l}(t) \cdot \dot{x}_{f2}(t) < 0 \quad \text{then } F_{dy,l}(t) &= F_{dy, \min} \end{aligned} \quad (12a)$$

$$\begin{aligned} \text{if } F_{d,u}(t) \cdot [\dot{x}_{f4}(t) - \dot{x}_{f2}(t)] > 0 \quad \text{then } F_{dy,u}(t) &= F_{dy, \max} \\ \text{if } F_{d,u}(t) \cdot [\dot{x}_{f4}(t) - \dot{x}_{f2}(t)] < 0 \quad \text{then } F_{dy,u}(t) &= F_{dy, \min} \end{aligned} \quad (12b)$$

where \dot{x}_{f2} and \dot{x}_{f4} are the velocities of the 2nd and 4th floor relative to the ground, and $F_{d,l}$ and $F_{d,u}$ are the force exerted by the frame on the lower and upper MR dampers, respectively, according to the scheme shown in Fig. 7. Operations of the semi-active devices according to the control algorithm shown above are independent of each other; in other words, any device can be operated autonomously by its sensors and electronics, which greatly simplifies the implementation of the control system.

Although characterized by a clear physical meaning, the adopted control algorithm can also be derived in the framework of the optimal control theory. For a dynamic system described in the state space by the equation $\dot{\mathbf{z}}(t) = \mathbf{f}[\mathbf{z}(t), \mathbf{u}(t)]$, a typical optimal control problem is the minimization of the following objective function:

$$J = \psi[\mathbf{z}(T)] + \int_0^T l[\mathbf{z}(t), \mathbf{u}(t)] dt \quad (13)$$

on a fixed time interval $0 \leq t \leq T$, with initial condition $\mathbf{z}(0) = \mathbf{z}_0$ and a set of allowable controls such as $\mathbf{u}(t) \in U$. That is, the problem is to find the control function $\mathbf{u}(t) \in U$ on $0 \leq t \leq T$, which leads to the smallest possible value of J and determines a unique state trajectory $\mathbf{z}(t)$ ($0 \leq t \leq T$) compatible with the system equation and the initial condition. This problem can be faced by the mathematical approach of multistage decision processes also known as dynamic programming (Luenberger 1979). For a linear system:

$$\dot{\mathbf{z}}(t) = \mathbf{A}\mathbf{z}(t) + \mathbf{B}\mathbf{u}(t) \quad (16)$$

whose objective functional is represented by the quadratic form:

$$J = \int_0^T l[\mathbf{z}(t), \mathbf{u}(t)] dt = \frac{1}{2} \int_0^T l[\mathbf{z}(t)^T \mathbf{Q}\mathbf{z}(t) + \mathbf{u}(t)^T \mathbf{R}\mathbf{u}(t)] dt \quad (17)$$

where \mathbf{Q} and \mathbf{R} are properly chosen matrices representing the relative weight given to the state versus the control action, the solution (i.e., the optimal control algorithm) can be derived by specifying to the linear system case (Eq. 16) the Hamilton-Jacobi-Bellman equation. The resulting optimal control law is given by:

$$\mathbf{u}_{opt} = -\mathbf{R}^{-1} \mathbf{B}^T \mathbf{P}\mathbf{z} \quad (18)$$

where $\mathbf{P}(t)$ is the solution of the Riccati equation:

$$\dot{\mathbf{P}} + \mathbf{Q} + \mathbf{P}\mathbf{A} + \mathbf{A}^T \mathbf{P} - \mathbf{P}\mathbf{B}\mathbf{R}^{-1} \mathbf{B}^T \mathbf{P} = 0 \quad (19)$$

However, dealing with structural control, it could be more interesting to minimize the instantaneous value of the objective rather than its integral over a given time interval. If we think to minimize the objective function between times t and $t + \Delta$, i.e., for $\Delta \rightarrow 0$ at every time instant t for all $0 \leq t \leq T$, the optimal control problem is referred to as 'instantaneous' (Yang and Akbarpour 1987, Yang *et al.* 1992) and the quadratic form shown above (Eq. 17) becomes:

$$J = l[\mathbf{z}(t), \mathbf{u}(t)] = \frac{1}{2}[\mathbf{z}(t)^T \mathbf{Q} \mathbf{z}(t) + \mathbf{u}(t)^T \mathbf{R} \mathbf{u}(t)] \quad (20)$$

By neglecting the relative importance of bounding the control actions ($\mathbf{R} = \mathbf{O}$), a simplified form of the instantaneous objective can be defined:

$$J = l[\mathbf{z}(t), \mathbf{u}(t)] = \frac{1}{2} \mathbf{z}(t)^T \mathbf{Q} \mathbf{z}(t) \quad (21)$$

and the instantaneous control problem becomes to find a minimum value of the objective at any time t :

$$J_{\min} = \min_{\mathbf{u} \in U} [J(t)] = \min_{\mathbf{u} \in U} \{l[\mathbf{z}(t), \mathbf{u}(t)]\} \quad (22)$$

With reference to the linear system described by Eq. (9), since it is not possible to directly modify the actual value of the objective function by $\mathbf{u}(t)$, the optimal control problem becomes to find the control function which guarantees J to be as decreasing as possible, by minimizing the contribution of $\mathbf{u}(t)$ to the time derivative of J :

$$\dot{J} = \mathbf{z}(t)^T \mathbf{Q} \dot{\mathbf{z}}(t) = \mathbf{z}(t)^T \mathbf{Q} \mathbf{A} \mathbf{z}(t) + \mathbf{z}(t)^T \mathbf{Q} \mathbf{e} \ddot{x}_g(t) + \mathbf{z}(t)^T \mathbf{Q} \mathbf{B} \mathbf{u}(t) = \dot{J}^z + \dot{J}^{\ddot{x}_g} + \dot{J}^u \quad (23)$$

where only the third part \dot{J}^u of \dot{J} may be instantaneously modified by properly choosing $\mathbf{u}(t)$.

The controllable part \dot{J}^u of \dot{J} reduces to the following expression:

$$\begin{aligned} \dot{J}^u &= [\mathbf{z}(t)^T \mathbf{Q} \mathbf{B}] \cdot \mathbf{u}(t) = [\mathbf{x}(t)^T \quad \dot{\mathbf{x}}(t)^T] \cdot \begin{bmatrix} \mathbf{Q}_{11} & \mathbf{Q}_{12} \\ \mathbf{Q}_{21} & \mathbf{Q}_{22} \end{bmatrix} \cdot \begin{bmatrix} \mathbf{O} \\ \mathbf{M}^{-1} \mathbf{a} \mathbf{l} \end{bmatrix} \cdot \mathbf{u}(t) = \\ &= [(\mathbf{x}^T \mathbf{Q}_{12} + \dot{\mathbf{x}}^T \mathbf{Q}_{22}) \cdot \mathbf{M}^{-1} \mathbf{a} \mathbf{l}] \cdot \mathbf{u}(t) \end{aligned} \quad (24)$$

It is worth to notice that the $n \times n$ matrices \mathbf{Q}_{11} and \mathbf{Q}_{21} ($n = 6$), obtained from the partition of the matrix $\mathbf{Q}_{2n \times 2n}$ are not influent within the control algorithm because they don't appear in Eq. (24).

If we choose $\mathbf{Q}_{12} = \mathbf{O}_{n \times n}$ and \mathbf{Q}_{22} as:

$$\mathbf{Q}_{22} = \begin{bmatrix} 0 & 0 & 0 & 0 & 0 & 0 \\ 0 & 1 & 0 & 0 & 0 & 1 \\ 0 & 0 & 0 & 0 & 0 & 0 \\ 0 & 0 & 0 & 1 & 0 & 0 \\ 0 & 0 & 0 & 0 & 0 & 0 \\ 0 & 0 & 0 & 0 & 0 & 0 \end{bmatrix}, \quad \mathbf{M} = \begin{bmatrix} 0 & 0 & 0 & 0 & 0 & 0 \\ 0 & m_{f2} & 0 & 0 & 0 & m_{bu} \\ 0 & 0 & 0 & 0 & 0 & 0 \\ 0 & 0 & 0 & m_{f4} & 0 & 0 \\ 0 & 0 & 0 & 0 & 0 & 0 \\ 0 & 0 & 0 & 0 & 0 & 0 \end{bmatrix} \quad (25)$$

the controllable part \dot{J}^u of \dot{J} is given by the following scalar expression:

$$\dot{J}^u = F_{d,l}^s(t) \cdot \dot{x}_{f2}(t) + F_{d,u}^s(t) \cdot (\dot{x}_{f4}(t) - \dot{x}_{f2}(t)) = -F_{d,l}(t) \cdot \dot{x}_{f2}(t) - F_{d,u}(t) \cdot (\dot{x}_{f4}(t) - \dot{x}_{f2}(t)) \quad (26)$$

Therefore, for the contribution \dot{J}^u of $\mathbf{u}(t)$ to the time derivative of J be minimum, the variable plastic threshold F_{dy} of the force in the lower and upper devices has to be set as shown in Eqs. (12a, 12b), which describe the algorithm adopted.

On the other hand, with the above choice of $\mathbf{Q} = \begin{bmatrix} \mathbf{O}_{n \times n} & \mathbf{O}_{n \times n} \\ \mathbf{O}_{n \times n} & \mathbf{Q}_{22} \end{bmatrix}$ and $\mathbf{R} = \mathbf{O}$, the objective function (20) to be minimized is somewhat linked to the kinetic energy of the dynamic system:

$$\begin{aligned} J &= \frac{1}{2} \mathbf{z}(t)^T \mathbf{Q} \mathbf{z}(t) = \frac{1}{2} [\mathbf{x}(t)^T \quad \dot{\mathbf{x}}(t)^T] \cdot \begin{bmatrix} \mathbf{O} & \mathbf{O} \\ \mathbf{O} & \mathbf{Q}_{22} \end{bmatrix} \cdot \begin{bmatrix} \mathbf{x}(t) \\ \dot{\mathbf{x}}(t) \end{bmatrix} = \frac{1}{2} \dot{\mathbf{x}}(t)^T \mathbf{Q}_{22} \dot{\mathbf{x}}(t) = \\ &= \frac{1}{2} m_{f2} \cdot \dot{x}_{f2}^2 + \frac{1}{2} m_{bu} \cdot \dot{x}_{bu} \cdot \dot{x}_{f2} + \frac{1}{2} m_{f4} \cdot \dot{x}_{f4}^2 \end{aligned} \quad (27)$$

The proposed control algorithm can be checked also from dynamic stability perspective, based on the exploitation of Lyapunov stability theory, usually adopted to check if an active control algorithm results in a stable system. The stability assessment involves the definition of a positive, real, scalar and lower bounded function V of the whole state \mathbf{z} . The Barbalat's Lemma can be used to demonstrate that, in a wide range of hypotheses, the negativeness of the time derivative dV/dt guarantees the system stability in the bounded input-bounded output sense. Thus, by adopting a function V equal to the objective J :

$$V = J = \frac{1}{2} \mathbf{z}(t)^T \mathbf{Q} \mathbf{z}(t) \quad (28)$$

the time derivative of V in the structural system described by Eq. (9) is:

$$\dot{V} = \mathbf{z}(t)^T \mathbf{Q} \dot{\mathbf{z}}(t) = \mathbf{z}(t)^T \mathbf{Q} \mathbf{A} \mathbf{z}(t) + \mathbf{z}(t)^T \mathbf{Q} \mathbf{e} \ddot{x}_g(t) + \mathbf{z}(t)^T \mathbf{Q} \mathbf{B} \mathbf{u}(t) \quad (29)$$

The only term that can be directly changed by the control action \mathbf{u} is the last one. Therefore, if \mathbf{u} is selected as shown in Eqs. (12a, 12b), its contribution to the time derivative of V , described by Eq. (29), is at any time as negative as possible. Therefore, the proposed algorithm cannot drive by itself the resulting controlled system to dynamic instability.

4. Analysis of the experimental results

The MISS frame mock-up has been tested on the shaking table using three different accelerograms, two natural and one artificial: the Tolmezzo (medium-rigid soil) record of the 1976 Friuli (Italy) earthquake, the second (N-S) component of the Northridge quake recorded in 1994 at the Sylmar County Hospital parking lot (California), and a synthetic accelerogram generated according to Eurocode 8 for soft (CGS) soil conditions. Fig. 8 shows the time-histories and the

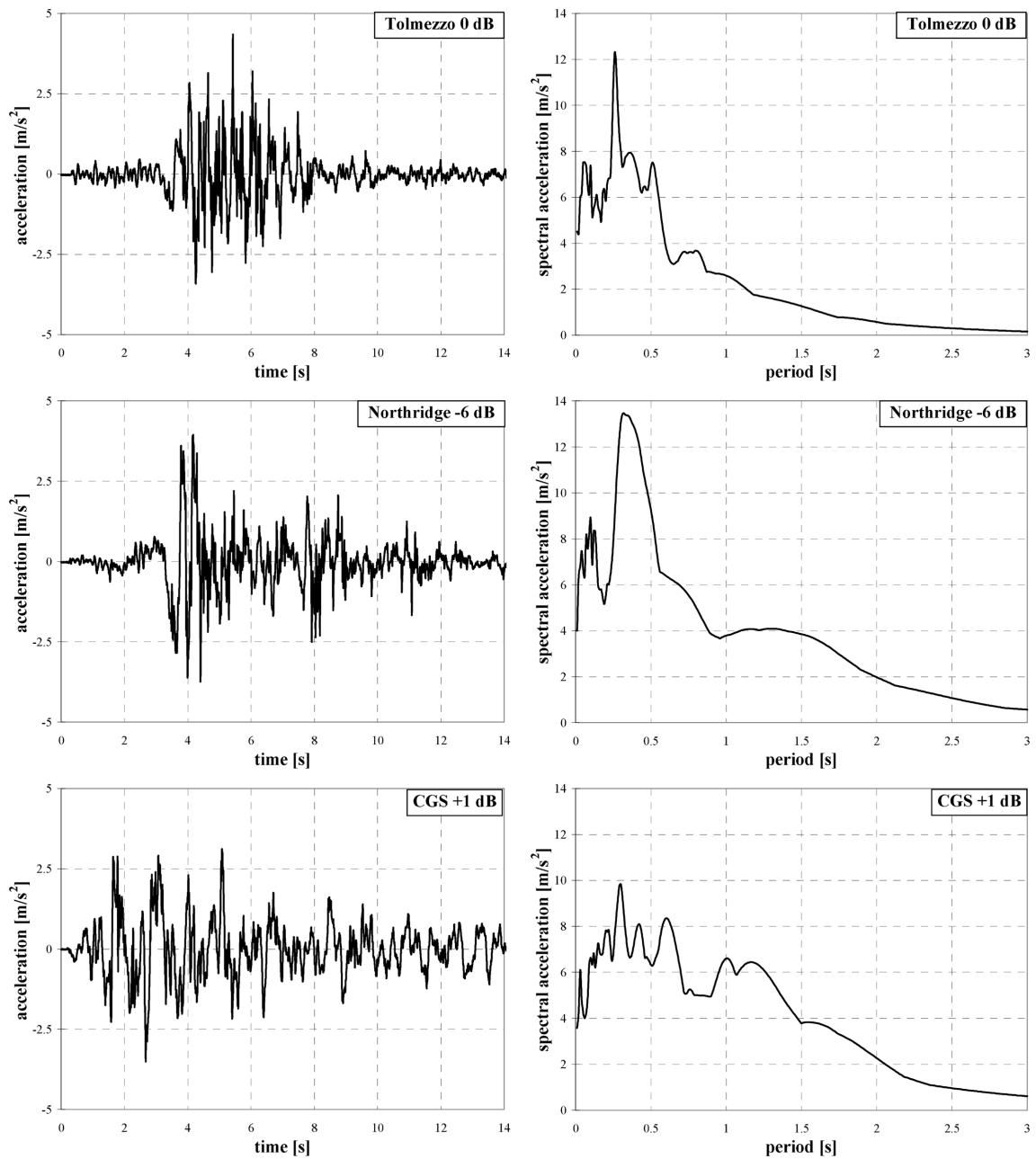


Fig. 8 Scaled time-histories and spectral acceleration (5% damping) of seismic inputs

acceleration response spectra (for 5% damping factor) of the considered seismic inputs, scaled down to the achieved maximum level.

The seismic tests have been performed in four different structural configurations: an uncontrolled, or unbraced, configuration (i.e., without MR dampers), a “passive off” control configuration (i.e., in absence of any control signal to MR dampers), a “passive on” (rigid link) control configuration (i.e.,

a constant 2.5 A current is provided to MR dampers), and a semi-active control configuration (i.e., the MR dampers are fed with a time-varying current input signal according to the algorithm). In the “passive off” configuration the MR dampers behave pretty much like viscous devices; in the “passive on” configuration, the MR dampers represent an almost rigid link between the braces and the hosting structure.

For each control configuration, the seismic inputs have been applied at increasing amplitudes (i.e., increasing levels expressed in dB) up to a maximum value corresponding to the achievement of a limit value of the 2nd floor displacement (20 mm) or of the table’s overturning moment (300 kNm). It is worth to note that the maximum level of the semi-active configuration is 2.5-4 times larger compared to the uncontrolled configuration.

4.1 Reduction of the structural response

Fig. 9 to 11 show the experimental results, in terms of peak 2nd floor relative displacement and peak 4th floor absolute acceleration, for all the control configurations and the input levels. Obviously, in comparison with the “passive off” case, reduced displacements and increased absolute

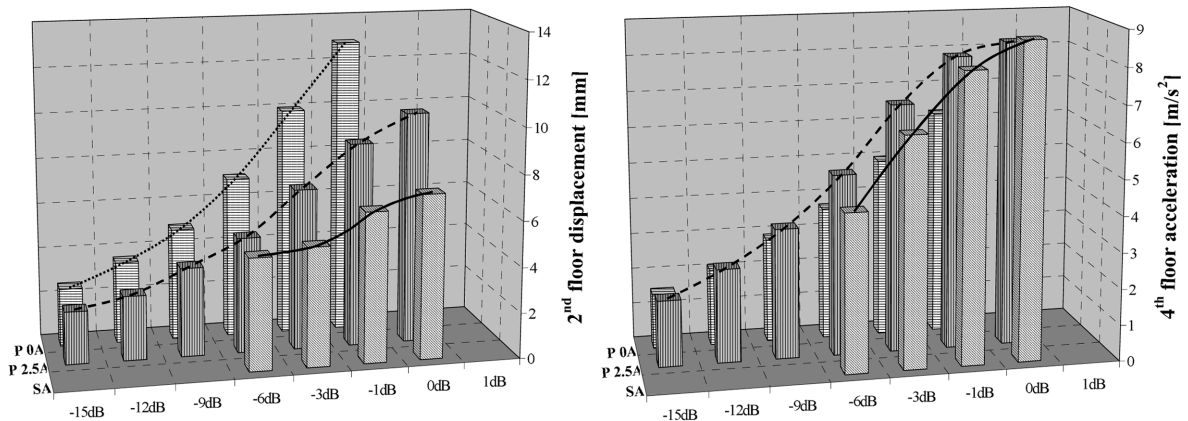


Fig. 9 Tolmezzo: relative displacement of the 2nd floor and absolute acceleration of the 4th floor

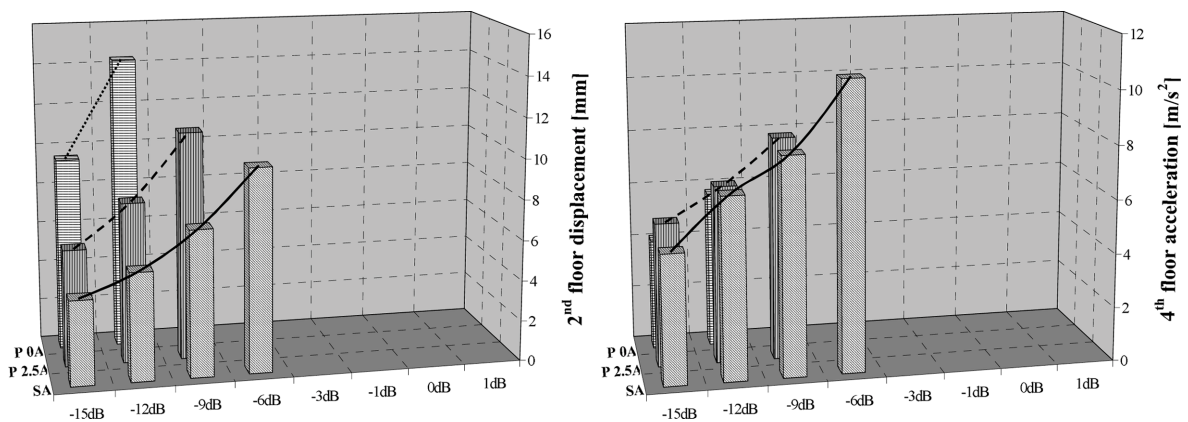


Fig. 10 Northridge: relative displacement of the 2nd floor and absolute acceleration of the 4th floor

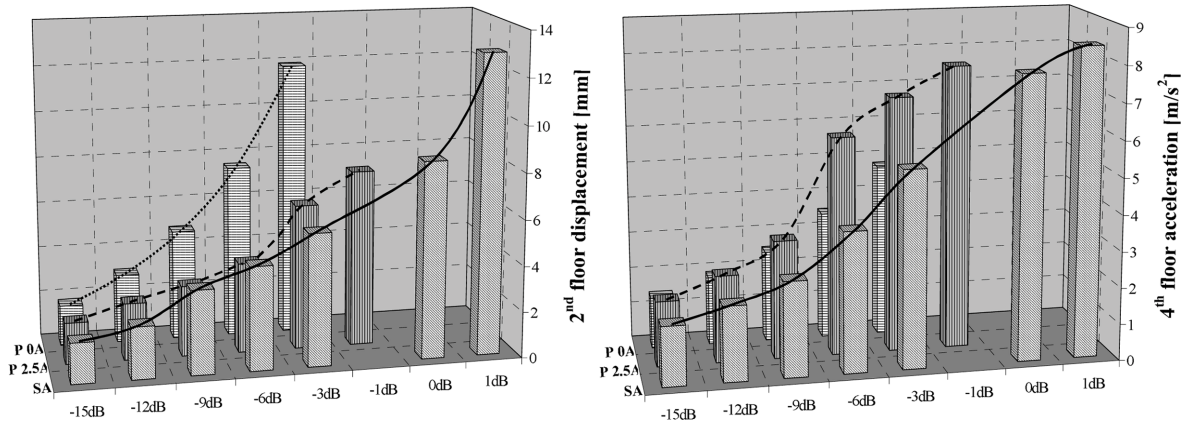


Fig. 11 CGS: relative displacement of the 2nd floor and absolute acceleration of the 4th floor

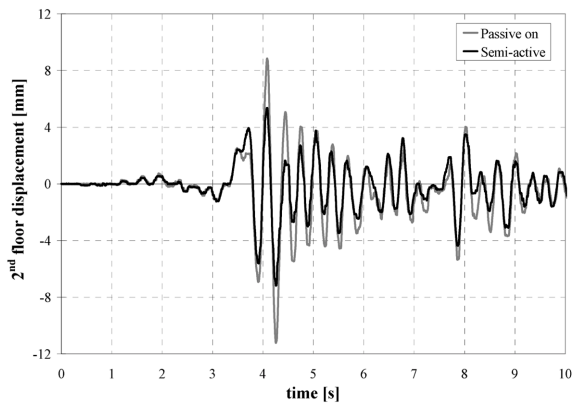


Fig. 12 Northridge -9 dB: relative displacement of the 2nd floor

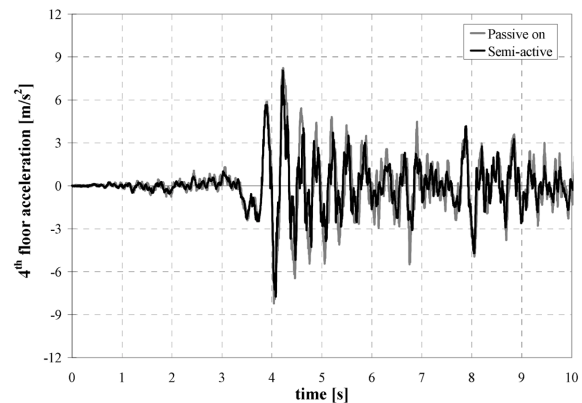


Fig. 13 Northridge -9 dB: absolute acceleration of the 4th floor

accelerations occur in the “passive on” configuration. On the contrary, however, in the semi-active configuration the recorded displacements show a reduction of about 30%-40% with respect to the “passive on” case, but the maximum accelerations appear very close to those recorded in the rigid link configuration. The figures also show that the amount of reduction of the response peaks (i.e., the effectiveness of the semi-active control system) is the higher the larger is the magnitude of the excitation.

The displacement response reduction and the trend of the acceleration can be observed in Figs. 12 and 13, reporting the time-histories of the MISS 2nd floor displacement and 4th floor acceleration for both “passive on” and semi-active configurations and for the Northridge -9 dB earthquake. The comparison of the two time-histories in Fig. 12 shows that the semi-active system allows not only a reduction of the peak displacements, but also a general improvement of the structural response.

Moreover, it is important to point out that the structural response in the “passive on” configuration appears to be strongly dependent on the input excitation, while the performance of the control system in the semi-active configuration has a quite weak dependence on the seismic input (Fig. 9 to 11).

4.2 Effectiveness through benchmark indexes

The effectiveness of the previously explained control strategy has been evaluated through the evaluation criteria proposed in the 3rd generation benchmark for seismically excited buildings (<http://cee.uiuc.edu/sst/benchmarks>). The following first three criteria, related to the building responses, have been considered:

$$J_1 = \max_{\substack{\text{Tolmezzo} \\ \text{Northridge} \\ \text{CGS}}} \left\{ \frac{\max_{t,i} \frac{|d_i(t)|}{h_i}}{\delta^{\max}} \right\} \quad (30)$$

$$J_2 = \max_{\substack{\text{Tolmezzo} \\ \text{Northridge} \\ \text{CGS}}} \left\{ \frac{\max_{t,i} |\ddot{x}_{ai}(t)|}{\ddot{x}_a^{\max}} \right\} \quad (31)$$

$$J_3 = \max_{\substack{\text{Tolmezzo} \\ \text{Northridge} \\ \text{CGS}}} \left\{ \frac{\max_t \left| \sum_i m_i \ddot{x}_{ai}(t) \right|}{F_b^{\max}} \right\} \quad (32)$$

J_1 is based on the peak interstory drift ratio (maximum drifts non-dimensionalized and normalized with respect to the associated floor height), where $d_i(t)$ is the interstory drift of the above-ground floors over the time-history of the earthquake, h_i is the height of each of the associated stories and $\delta^{\max} = \max_{i,t} \{d_i(t)/h_i\}$ is the maximum interstory drift ratio of the uncontrolled structure. J_2 is based on the maximum floor accelerations non-dimensionalized by the maximum uncontrolled floor acceleration, where $\ddot{x}_{ai}(t)$ and \ddot{x}_a^{\max} are the absolute accelerations of the i -th level with and without control devices. J_3 is based on the maximum base shear non-dimensionalized by the maximum uncontrolled base shear, where m_i is the seismic mass of the i -th above-ground floor and F_b^{\max} is the maximum base shear of the uncontrolled structure.

Then, the following two criteria, assessing the required performance of the control devices, have been analyzed:

$$J_{11} = \max_{\substack{\text{Tolmezzo} \\ \text{Northridge} \\ \text{CGS}}} \left\{ \frac{\max_{t,l} |f_l(t)|}{W} \right\} \quad (33)$$

$$J_{12} = \max_{\substack{\text{Tolmezzo} \\ \text{Northridge} \\ \text{CGS}}} \left\{ \frac{\max_{t,l} |y_l^a(t)|}{x^{\max}} \right\} \quad (34)$$

J_{11} is based on the maximum control force $f_l(t)$ generated by the l -th control device over the time-history of the earthquake, where W is the seismic weight of the building based on the above-ground mass of the structure. J_{12} is based on the maximum stroke $y_l^a(t)$ of the l -th control device non-

Table 3 Evaluation criteria for the controlled MISS structure

Control configuration	Evaluation criterion		
	Passive off	Passive on	Semi-active
Interstory drift ratio (J_1)	0.397	0.247	0.212
Level acceleration (J_2)	0.500	0.812	0.637
Base shear (J_3)	0.534	0.762	0.650
Control force (J_{11})	0.007	0.061	0.064
Control device stroke (J_{12})	0.318	0.042	0.093

dimensionalized by the maximum uncontrolled displacement relative to the ground x^{\max} of the various floors of the structure. Table 3 shows the values of the evaluation criteria applied to the MISS frame structure in the “passive off”, “passive on” and semi-active configurations. The value of each criterion in one of the three control configurations represents the maximum of the values computed under the earthquakes Tolmezzo -1 dB, Northridge -12 dB and CGS -3 dB. At these amplitudes, experimental data were available for all the configurations tested, whereas some of the passive configurations could not be tested, for safety reasons, at higher amplitudes.

4.3 Dissipated energy

The behaviour of the semi-active control system can be interpreted from an energy balance perspective, by deriving from the equation of motion of the system (Eq. 7) the following energy balance:

$$E_e(t) + E_k(t) + E_d(t) = E_i(t) \quad (35)$$

where $\mathbf{x}_t = \mathbf{x} + \mathbf{x}_g$, $E_e(t) = 0.5 \cdot \mathbf{x}^T \cdot \mathbf{K} \cdot \mathbf{x}$ is the elastic stored energy, $E_k(t) = 0.5 \cdot \dot{\mathbf{x}}_t^T \cdot \mathbf{M} \cdot \dot{\mathbf{x}}_t$ is the kinetic energy, $E_i(t) = \int_0^t \dot{\mathbf{x}}_t^T \cdot \mathbf{M} \cdot d\mathbf{x}_g$ is the seismic input energy, and E_d is the dissipated energy. In the passive

off configuration of the tested building, under the action of the Tolmezzo earthquake base acceleration, a total energy of about 7 kJ was input into the structure (Fig. 14). Most of this energy was damped out by the MR dampers in their passive, 0 A state, but a peak of about 2 kJ of elastic+kinetic energy was reached many times in the strongest phase of the base excitation. In both the passive on and semi-active configurations of the control system, the total input energy reduced to about 5 kJ. This is in agreement with the trend of the input energy spectra of recorded earthquakes, whose ordinates usually increase almost linearly with the period T of the structure, for $T < 1$ s (De Luca and Serino 1988). However, the sum of elastic + kinetic energy reached a peak of about 2 kJ in the passive on configuration and a maximum value of about 1.5 kJ during semi-active operations. In other words, the particular semi-active logic adopted to drive the MR dampers did not change the global dynamic behaviour of the structure, compared to a rigid-linked bracing system but, forcing the damping phases in selected time intervals, was successful in optimizing the amount of energy dissipated.

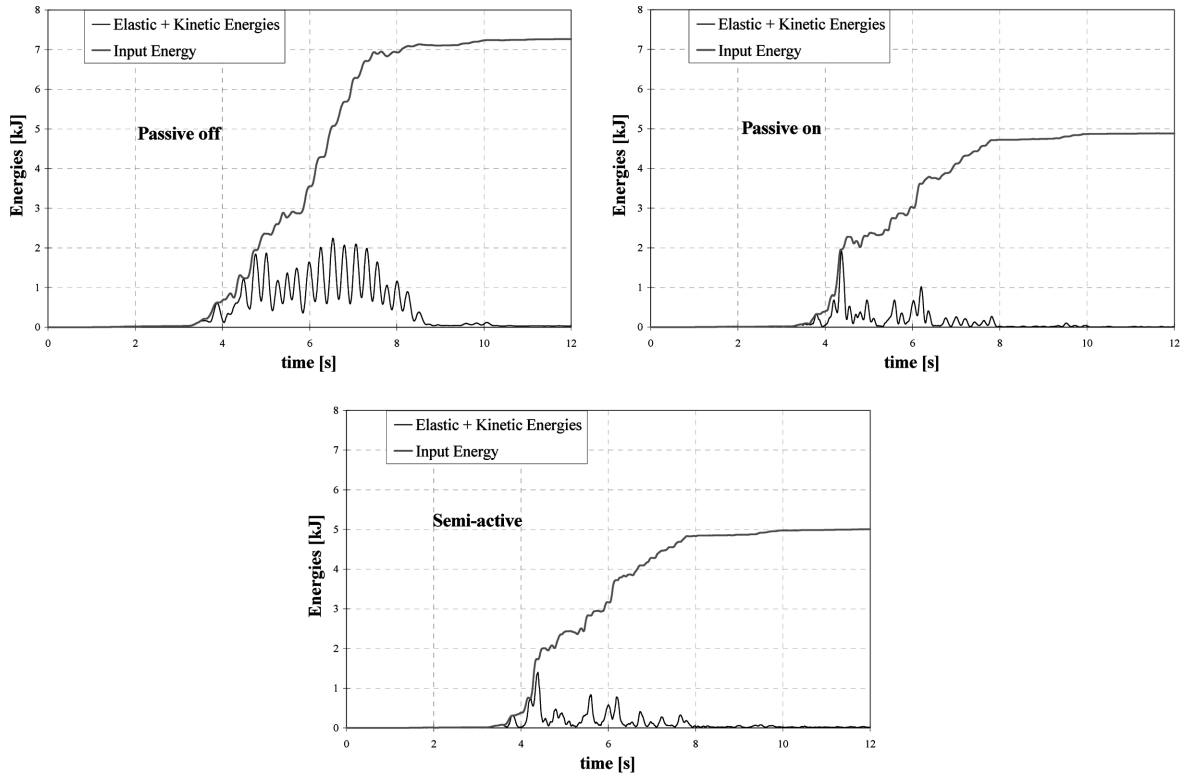


Fig. 14 Comparison of energies corresponding to different configurations

4.4 Operating delays

The control chain (acquisition-processing-actuation) of the semi-active bracing system is characterized by time delays, as described in the following:

- a time delay of the control electronics τ_c , which includes, consecutively, the time intervals associated to signal acquisition, to acquired signal processing through the algorithm and to operations of the power supply, the latter being the time interval starting when the driving signal (in output from the algorithm and in input to the power supply) is issued and ending when the current (in output from the power supply and in input to the MR damper) begins to change;
- a time delay of the electrical part of the damper (or of its electromagnetic circuit) τ_e , which is the time interval starting when the current (in input to the device) begins to change and ending when the current reaches the commanded nominal value within a $\pm 5\%$ tolerance;
- a time delay of the mechanical part of the damper τ_m , representing the time interval between the instant when the current (in input to the device) begins to change and the instant when the damper begins to react, i.e., begins to adjust its mechanical behaviour.

Fig. 15, aiming to show the promptness of the semi-active MR device, reports a magnification of some time histories recorded during the seismic test performed under Northridge -9 dB earthquake. The recorded signals are the displacement of the 2nd floor x_{f2} , the relative displacement of the damper's ends $x_{f2} - x_{b1}$, the force developed by the device F_d , the driving signal c and the current i inside the damper. The time delay τ_c of the control electronics, which spans from the moment in

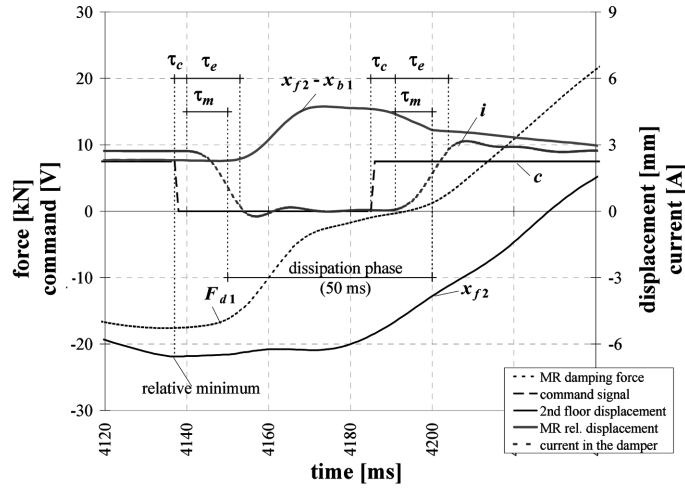


Fig. 15 Semi-active operation of the MR damper: seismic test under Northridge -6 dB

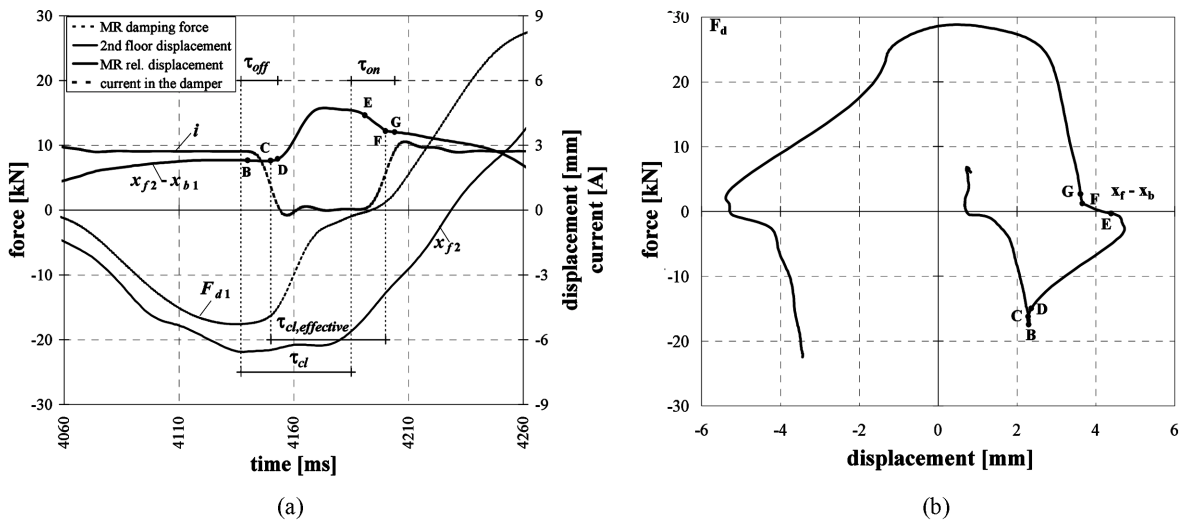


Fig. 16 Semi-active operation in seismic test under Northridge -6 dB

which the product in Eq. (11) changes its sign to negative to the moment when the command signal is issued, turned out to be variable but an upper bound of about 6 ms was found for both the on-off and the off-on phases (the delay of the power supply is within 5 ms in both phases). It is worth to note that the delay τ_c was associated to the adoption of commercial hardware and software and, therefore, could be further shortened by using purposefully manufactured electronics. The delay τ_e of the electromagnetic circuit, spanning from the issue of the command signal to the stabilization of the current into the damper at its nominal value, is within 13 ms in both the on-off and the off-on phases. The mechanical delay τ_m of the MR damper measures the time from the control signal to the moment where the damper adjust its behaviour according to the command received. The end of the mechanical delay can be found as a discontinuity of the damper's relative displacement. The mechanical delay turned out to be shorter than the electric delay and its typical value was 10 ms.

In Fig. 16, to better understand the MR damper's behaviour during semi-active operations, the path described in the force-displacement plane (Fig. 16b) has been underlined by the points marked with capital letters from B to F on the time-history of the MR damper displacement (Fig. 16a). These key points are described in the following:

- B** – Following a relative minimum of the 2nd floor's displacement and a switch off command (0 V) to the device, the current begins to decrease, which will cause the start of a sharp change of the force in the damper. This is the beginning of the dissipation activity of the semi-active device.
- C** – The MR damper begins to react before the current inside the damper reaches the commanded value (0 A).
- D** – The current reaches the nominal commanded value within a tolerance $\pm 5\%$. From this point, the relative displacement of the MR damper increases whereas the force inside the device reduces gradually to 0.
- E** – The elastic springs have dissipated all the stored energy and, after a switch on command (7.5 V) issued by the algorithm to the device, the current begins to increase and the springs start to accumulate elastic energy again.
- F** – The MR damper begins to stop before the current inside the damper reaches the commanded value (3 A).
- G** – The current reaches the 95% of the maximum value commanded by the algorithm (3 A), the damper is at rest, the springs keep accumulating elastic energy.

In Fig. 16(a) τ_{off} and τ_{on} are the total time delays, i.e., the time intervals required by the current to reach 5% and 95% of the nominal value set by the algorithm, starting from the time when the product in Eq. (11) changes its sign, respectively in the on-off and the off-on phase. These delays have been measured at any occurrence of the operational cycle of the controlling algorithm and for all of the tests performed. A statistical analysis of such data allows to conclude that the delays τ_{off} and τ_{on} are practically independent on the test frequency and their mean values are about 16 ms in the on-off phase and about 19 ms in the off-on phase. Finally, in the same Fig. 16(a) τ_{cl} is the commanded operation time decided by the algorithm and $\tau_{cl, effective}$ is the time interval comprising the beginning and the end of the 0 A phase of the semi-active damper. Therefore, τ_{cl} and $\tau_{cl, effective}$ provide location and represent duration of theoretical and effective semi-active operations, respectively. As shown in figure, τ_{cl} and $\tau_{cl, effective}$ have approximately the same duration and are offset by about 13 ms.

5. Numerical-experimental comparison

The effectiveness of the 4+2-DOF numerical model presented before has been checked through experimental-numerical comparisons. The numerical model, described by Eqs. (7) to (10), is shown in Fig. 17. Fig. 18 shows a comparison of experimental and numerical results corresponding to a the "passive on" configuration and to the Northridge acceleration record scaled down at -12 dB and demonstrates a satisfactorily agreement between numerical and experimental data.

The numerical model has been utilized in a parametric analysis aiming to test virtual passive devices able to improve the performances of the experimental system. The virtual passive devices have been selected so as to minimize the peak displacements of the main structure and from this perspective have been considered optimal. The experimental data have been compared to numerical

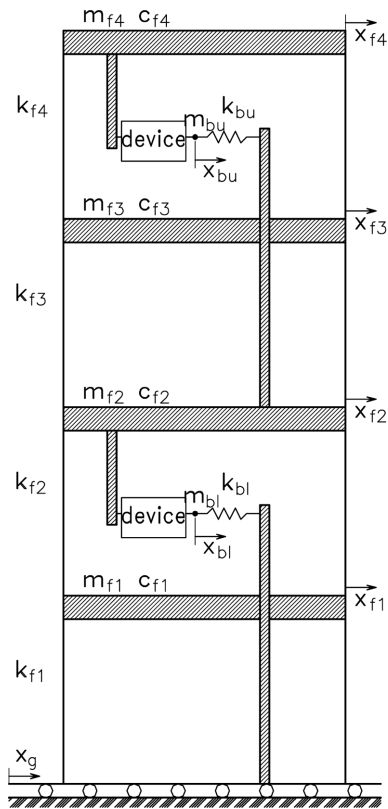


Fig. 17 Six degree of freedom model of MISS structure

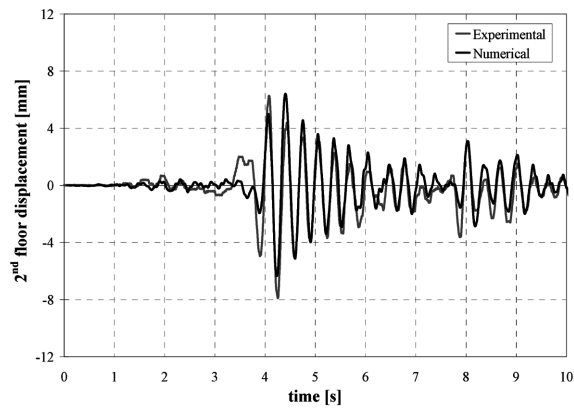


Fig. 18 Passive on configuration with Northridge -12 dB

results associated to the following virtually optimal passive devices:

- linear viscous dampers, ($C_d = 350$ kNs/m);
- friction-like dampers ($F_{dy} = 15$ kN);
- passive MR damper ($C_d = 300$ kNs/m, $F_{dy} = 2.5$ kN).

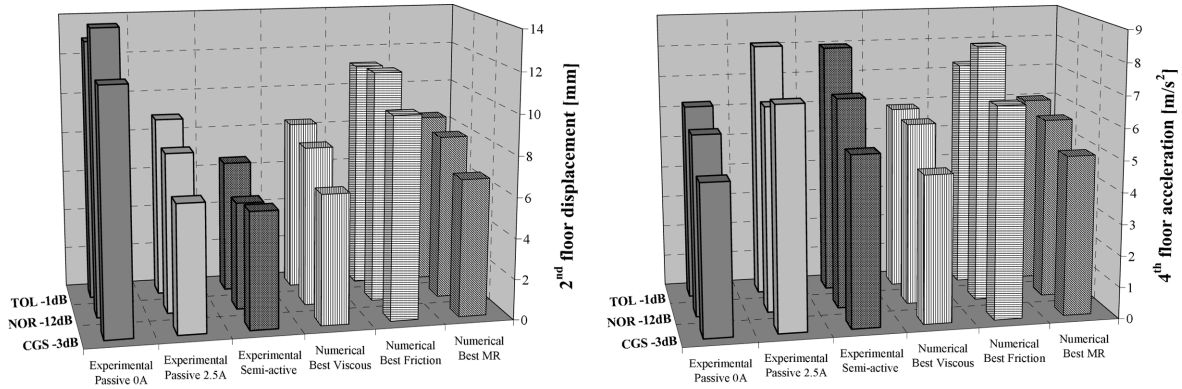


Fig. 19 Experimental-numerical comparison

Fig. 19 shows the comparison of the experimental and numerical results in terms of peak relative displacements and absolute accelerations. As for displacements, Fig. 19 shows that the proposed experimental semi-active control system outperforms any other passive device, either real or numerical.

6. Conclusions

The experimental testing campaign on a structural model equipped with semi-active MR dampers allowed to deepen the knowledge on the adoption of such devices in the context of semi-active control of civil structures.

A very simple control algorithm based on a clear physical meaning turned out to be appropriate to control in real time the behaviour of the semi-active dampers adopted in the experimental test. Its implementation has been feasible using commercial hardware and software.

The reduction of the structural response associated to the proposed semi-active control system has been checked both in terms of peak values of displacements and accelerations and in terms of a general improvement of the response time histories. The efficiency of the proposed control system has been evaluated also in terms of the performances indexes widely utilized in the structural control community.

An energy analysis of the experimental data has shown that the proposed control system achieves a better efficiency in damping out the energy flowing from a ground motion compared to passive dissipation systems.

A comprehensive analysis of the operating delays of the control system has shown that, dealing with magnetorheological dampers properly driven, these delays can be bounded in the range 10 to 15 ms.

Finally, a numerical model able to reproduce the experimental data has been utilized for a parametric investigation aimed to numerically tests many different passive devices, whose best performances has been compared to those experimentally obtained by the proposed control system.

Acknowledgements

The research has been performed within the SPACE project (Semi-active and PASSive Control of the dynamic behaviour of structures subjected to Earthquakes, wind and vibrations), funded by the European Commission (5th FP, 1998-2002), Contract EVG1-CT-1999-00016. The authors would like to thank all the partners of the project: Maurer Söhne GmbH & Co. KG (D) for the manufacturing of MR devices; Bilfinger Berger Aktiengesellschaft (D) for the help in the design of the control device; Thales Underwater Systems (F) for the realization of the electronics of the control system; Kungl Tekniska Högskolan (S), for the study of MR fluids; ENEL.Hydro – ISMES (I) for the tests on the MR devices and the shaking table tests; ENEA, Ente per le Nuove Tecnologie, l'Energia e l'Ambiente (I) for making available the MISS mock-up and the design of its modifications; CESI (I); Tun Abdul Razak Research Centre (UK).

References

- Chen, Z.Q., Wang, X.Y., Ko, J.M., Ni, Y.Q., Spencer, B.F., Yang, G. and Hu, J.H. (2004), "MR damping system for mitigating wind-rain induced vibration on Dongting Lake Cable-Stayed Bridge", *Wind and Structures*, **7**(5), 293-304.
- Chu, S.Y., Soong, T.T., Reinhorn, A.M., Helgeson, R.J. and Riley, M.A. (2002), "Integration issues in implementation of structural control systems", *J. Struct. Control*, **9**, 31-58.
- De Luca, A. and Serino, G. (1988), "L'approccio energetico nella progettazione sismica", *Ingegneria Sismica*, Anno, **V**(3), 18-27 (in Italian).
- Hiwatashi, T., Shiozaki, Y., Fujitani, H., Iiba, M., Tomura, T., Sodeyama, H. and Soda, S. (2002), "Semi-active control of large-scale test frame by magneto-rheological damper", *Proc. 3rd World Conf. on Structural Control*, ed F Casciati, United Kingdom: Wiley, 2, 355-360.
- Inaudi, J.A. and Hayen, J.C. (1995), "Research on variable-structure systems in the United States", *Proc. Post-SMiRT Conf. Sem. on Seismic Isolation, Passive Energy Dissipation and Control of Vibrations*, Santiago, Chile: GLIS, 591-622.
- Inaudi, J.A. (2000), "Performance of variable-damping systems: Theoretical analysis and simulation", *Proc. 3rd Int. Workshop on Structural Control*, ed F Casciati & Magonette, United Kingdom: World Scientific, 301-316.
- Jung, H.J., Spencer, B.F., Ni, Y.Q. and Lee, I.W. (2004), "State-of-the-art of semiactive control systems using MR fluid dampers in civil engineering applications", *Struct. Eng. Mech.*, **17**(3), 493-526.
- Kobori, T. (2002), "Past, present and future in seismic response control of civil engineering structures", *Proc. 3rd World Conf. on Structural Control*, ed F Casciati, United Kingdom: Wiley, 1, 9-14.
- Luenberger, D.G. (1979), *Introduction to Dynamic Systems - Theory, Models & Applications*, John Wiley & Sons Inc., USA.
- Medeot, R., Braun, C., Seiler, C., Debost, S., Hedin, F., Bergamo, G., Forni, M., Bettinali, F., Serino, G. and Fuller, K.N.G. (2001), "The EC-funded project SPACE (Semi-Active and Passive Control of the Dynamic Behavior of Structures Subjected to Earthquakes, Wind and Vibrations)", *Proc. 7th Int. Seminar on Seismic Isolation, Passive Energy Dissipation and Active Control of Vibrations of Structures*, Assisi, Italy: GLIS, 1, 447-475.
- Morishian, S., Shiraishi, T. and Nakaya, N. (2002), "Adaptive vibration control of a structure using MR damper", *Proc. 3rd World Conf. on Structural Control*, ed F Casciati, United Kingdom: Wiley, 3, 761-766.
- National Instruments (2000), *LabVIEW™ – User Manual*, National Instruments Corp., Austin, Texas – USA.
- Nishitani, A. and Inoue, Y. (2001), "Overview of the application of active/semiactive control to building structures in Japan", *Earth. Eng. Struct. Dyn.*, **30**, 1565-1574.
- Occhiuzzi, A. and Serino, G. (2002), "Control strategies for semi-active structural control devices", *Proc. 3rd World Conf. on Structural Control*, ed F Casciati, United Kingdom: Wiley, 3, 641-647.
- Occhiuzzi, A. and Spizzuoco, M. (2003), "Semi-active magnetorheological dampers applied to a steel building",

- Proc. Forth Int. Conf. on Behaviour of Steel Structures in Seismic Areas*, ed F M Mazzolani, The Netherlands: Balkema, 633-639.
- Occhiuzzi, A., Spizzuoco, M. and Serino, G. (2003), "Experimental analysis of magnetorheological dampers for structural control", *Smart Mater. Struct.*, **12**, 703-711.
- Serino, G., Occhiuzzi, A., Spizzuoco, M., Seiler, C. and Fischer, O. (2002), "Semi-active control via MR dampers: Algorithms, numerical modeling and prediction of the resulting response of structures", *Proc. 3rd World Conf. on Structural Control*, ed F Casciati, United Kingdom: Wiley, 2, 1113-1118.
- Spencer, B.F. and Nagarajaiah, S. (2003), "State of the art of structural control", *J. Struct. Engrg.*, **129**, 845-856.
- Symans, M.D. and Constantinou, M.C. (1999), "Semi-active control systems for seismic protection of structures: A state-of-the-art review", *Eng. Struct.*, **21**, 469-487.
- Tagami, J., Koshida, H., Kurino, H., Sugiyama, T., Suwa, M. and Mori, F. (2002), "Forced vibration test of an 11-storey building with semi-active switching oil damper", *Proc. 3rd World Conf. on Structural Control*, ed F Casciati, United Kingdom: Wiley, 2, 75-80.
- University of Illinois Urbana-Champaign – Department of Civil and Environmental Engineering <http://cee.uiuc.edu/sstl/benchmarks>
- Wongprasert, N. and Symans, M.D. (2002), "Experimental evaluation of a smart base-isolation system consisting of spherical sliding bearings and variable fluid dampers", *Proc. 3rd World Conf. on Structural Control*, ed F Casciati, United Kingdom: Wiley, 2, 331-336.
- Yamamoto, M., Higashino, M. and Aizawa, S. (2002), "Development of semi-active mass damper system using oil damper with solenoid valves", *Proc. 3rd World Conf. on Structural Control*, ed F Casciati, United Kingdom: Wiley, 2, 343-348.
- Yang, G., Spencer, B.F., Carlson, J.D. and Sain, M.K. (2002), "Large-scale MR fluid dampers: Modeling and dynamic performance considerations", *Eng. Struct.*, **24**, 309-323.
- Yang, N.J. and Akbarpour, A. (1987), "New optimal control algorithms for structural control", *J. Eng. Mech.*, **113**, 1369-1386.
- Yang, N.J., Li, Z. and Liu, S.C. (1992), "Stable controllers for instantaneous optimal control", *J. Eng. Mech.*, **118**, 1612-1630.